Acta Radiologica
2020, Vol. 61(12) 1668–1676

DOI: 10.1177/0284185120909337
journals.sagepub.com/home/acr


Visualizing the autonomic and somatic innervation of the female pelvis with 3D MR neurography: a feasibility study

Katja N De Paepe[1,2], David M Higgins[3], Iain Ball[4], Veronica A Morgan[2], Desmond P Barton[5] and Nandita M deSouza[1,2]

Abstract

Background: Treatment of female pelvic malignancies often causes pelvic nerve damage. Magnetic resonance (MR) neurography mapping the female pelvic innervation could aid in treatment planning.

Purpose: To depict female autonomic and somatic pelvic innervation using a modified 3D NerveVIEW sequence.

Material and Methods: Prospective study in 20 female volunteers (n = 6 normal, n = 14 cervical pathology) who underwent a modified 3D short TI inversion recovery (STIR) turbo spin-echo (TSE) scan with a motion-sensitive driven equilibrium (MSDE) preparation radiofrequency pulse and flow compensation. Modifications included offset independent trapezoid (OIT) pulses for inversion and MSDE refocusing. Maximum intensity projections (MIP) were evaluated by two observers (Observer 1, Observer 2); image quality was scored as 2 = high, 1 = medium, or 0 = low with the sciatic nerve serving as a reference. Conspicuity of autonomic superior (SHP) and bilateral inferior hypogastric plexuses (IHP), hypogastric nerves, and somatic pelvic nerves (sciatic, pudendal) was scored as 2 = well-defined, 1 = poorly defined, or 0 = not seen, and inter-observer agreement was determined.

Results: Images were of medium to high quality according to both observers agreeing in 15/20 (75%) of individuals. SHP and bilateral hypogastric nerves were seen in 30/60 (50%) of cases by both observers. Bilateral IHP was seen in 85% (34/40) by Observer 1 and in 75% (30/40) by Observer 2. Sciatic nerves were well identified in all cases, while pudendal nerves were seen bilaterally by Observer 1 in 65% (26/40) and by Observer 2 in 72.5% (29/40). Agreement between observers for scoring nerve conspicuity was in the range of 60%–100%.

Conclusion: Modified 3D NerveVIEW renders high-quality images of the female autonomic and pudendal nerves.

Keywords

Magnetic resonance imaging, peripheral nerves, female, pelvis, autonomic, somatic

Date received: 25 November 2019; accepted: 21 January 2020

Introduction

Treatment of pelvic malignancies commonly affects the somatic and autonomic pelvic innervation and may critically influence a patient's quality of life. The close proximity of nerve plexuses to the uterus and ovaries means that, despite the implementation of nerve-sparing techniques (1–3), surgery for primary gynecological cancers often causes injury of the pelvic plexuses (4–8), resulting in early and late complications, most often related to bladder function (9). Postoperative sexual (10) and anorectal dysfunction have also been reported. Additionally, in recurrent

[1]The Institute of Cancer Research, Division of Radiotherapy and Imaging, Sutton, UK
[2]The Royal Marsden NHS Foundation Trust, Department of Radiology, London, UK
[3]Philips, Guildford, UK
[4]Philips, Sydney, Australia
[5]The Royal Marsden NHS Foundation Trust, Department of Gynecological Oncology, London, UK

Corresponding author:
Katja N De Paepe, The Royal Marsden NHS Foundation Trust, Department of Radiology, 15 Cotswold Road, Sutton, London SM2 5NG, UK.
Email: katjadepaepe@gmail.com

gynecological malignancy involving the pelvic side wall, accurate assessment of tumor location relative to the sciatic nerve is of utmost importance to determine whether patients are suitable for salvage surgery such as exenteration (11). When irradiation is considered, there is an increasing move towards sciatic nerve-sparing radiotherapy (12), mandating clear depiction of the entire trajectory of the sciatic nerve.

To date, magnetic resonance neurography (MRN) has been used to depict the lumbosacral plexus and some of its larger somatic branches (13,14). However, imaging the autonomic pelvic nerves poses more of a challenge. The fine, mesh-like organization of the plexuses hampers their identification and differentiation from adjacent vessels and viscera. As a result, few imaging studies have been able to visualize the pelvic autonomic innervation, and there is only one in vivo study where segmentation of these plexuses using post-processing of a three-dimensional (3D) sequence has been addressed (15). Direct and reliable visualization of the autonomic and somatic pelvic nerves by optimizing the data acquisition could facilitate primary and salvage surgery, as well as radiotherapy planning, and may improve post-treatment morbidity. The purpose of this study, therefore, was to modify and optimize an existing heavily T2-weighted (T2W) 3D sequence (NerveVIEW, designed for brachial and lumbar plexus) and assess its use for the identification of pelvic autonomic (superior hypogastric plexus, hypogastric nerves, inferior hypogastric plexus) and somatic (sciatic, pudendal) nerves at 3 T.

Material and Methods

Participants

This prospective study was approved by the local ethical committee for sequence development and evaluation and written consent was obtained from all participants. Any female volunteers or patients aged >18 years without previous pelvic surgery or other conditions likely to affect pelvic anatomy (e.g. endometriosis) or metallic implants/intrauterine contraceptive devices were eligible. Additional exclusion criteria were general contraindications to MR imaging (MRI) (e.g. claustrophobia). The MRN sequence was applied in six healthy female volunteers (age range = 32–60 years; mean age = 46 years), as well as in 14 patients (age range = 25–63 years; mean age = 38 years) with focal cervical pathology. Of these patients, two had cervical intra-epithelial neoplasia (CIN) and 12 had cervical cancer (stage 1b, n = 10; stage 2b (limited), n = 2). The patients with cervical cancer were part of a larger unrelated study. In the patient cohort, no malignant involvement of the adjacent neurovascular bundles was present on T2W images. All participants were asked to empty their bladders before imaging.

Imaging technique and protocol modification

All scans were performed on a 3.0-T Philips Achieva TX (Best, the Netherlands) using a TorsoXL receiver array. The standard NerveVIEW sequence is a heavily T2W turbo spin-echo (TSE), providing a large 3D field of view (FOV) with a small voxel size. It uses extended echo trains with variable flip angle (FA) refocusing sweeps, so that magnetization is preserved for later in the echo train, enabling higher isotropic resolution. Strong T2-weighting is created with motion-sensitive driven equilibrium (MSDE) preparation, to increase nerve contrast, incorporating flow compensation gradients to suppress signal from veins. Short TI inversion recovery (STIR) is used to suppress fat signal. Pulse sequence details include: acquired voxel resolution = $1.1 \times 1.1 \times 2.0$ mm; repetition time (TR)/equivalent echo time (TEequiv) = 2300/176 ms; TSE factor = 51; FOV = 324 mm; 150 slices; total SENSitivity Encoding (SENSE) acceleration = 3.75. The MSDE T2 prep time was 23.7 ms to attain adequate fat and vascular suppression. A velocity encoding (VENC) of 2 cm/s was set for the MSDE flow compensation gradients; this was optimized for the female pelvis before implementation in study participants. The STIR inversion time (TI) was 280 ms. The scan time was 6 min 33 s.

An important sequence modification which allowed better visualization of pelvic nerves was the introduction of offset independent trapezoid (OIT) pulses (16) for the STIR inversion and for the MSDE refocusing pulses. The OIT pulses used in this work have a larger transmit bandwidth (STIR pulse = 15 kHz; MSDE refocusing = 6.5KHz) for improved B0 insensitivity over a large FOV versus conventional hyperbolic secant inversion. Further modifications to NerveVIEW were the following: the use of 3D non-selective refocusing pulses for the TSE readout to shorten the echo-spacing; the use of a hybrid profile order in which both ky and kz varied within one turbo shot readout; and tailoring the refocusing sweep to reduce to a FA of 25° before increasing to a plateau of 110°, which provides a signal plateau of about 200 ms to adequately sample the 80–90 ms long T2 component of nerve signal biexponential decay. Comparison with the standard NerveVIEW and the modified NerveVIEW is summarized in Table 1 and an example of the image quality of both sequences intended for pelvic nerve imaging is illustrated in Fig. 1.

Table 1. Comparison of parameters between standard and modified NerveVIEW.

	Standard NerveVIEW	Modified NerveVIEW
Orientation	Coronal	Coronal
Acquired voxel (mm)	$1.1 \times 1.1 \times 2.0$	$1.1 \times 1.1 \times 2.0$
Field of view (mm)	$250 \times 324 \times 150$	$250 \times 324 \times 150$
Slices	150	150
TR (ms)	2200	2300
TEequiv (ms)	180	176
TSE factor	56	51
Refocusing pulses	Constant	Tissue-specific (nerve)
Min angle (°)	50	25
Max angle (°)	50	110
Fat suppression	SPAIR	STIR
Inversion recovery delay (ms)	210	280
Pulse type	NA	OIT broad adiabatic
MSDE		
Refocusing type	Conventional adiabatic	OIT broad adiabatic
VENC (cm/s)	0.5	2
TEprep pulse	50	23.7
Time	5 min 43 s	6 min 33 s

MSDE, motion-sensitive driven equilibrium; NA, not applicable; OIT, offset independent trapezoid; SPAIR, SPectral Attenuated Inversion Recovery; STIR, short TI inversion recovery; TEequiv, echo time equivalent; TEprep, echo time preparation; TR, repetition time; TSE, turbo spin echo; VENC, velocity encoding.

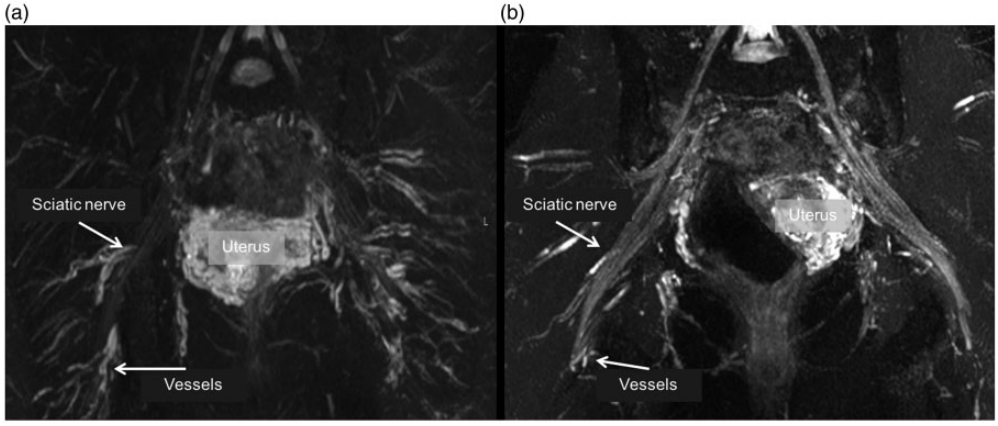

Fig. 1. A 45-year-old female volunteer. The standard 3D NerveVIEW image (a) and the modified 3D NerveVIEW image (b) demonstrates that the implemented modifications increased the signal of the nerves and provided better vascular signal suppression.

Image and statistical analysis

From the native images, maximum intensity projection (MIP) images were rendered on a Philips Extended Workstation to enable selection of slab thickness (3–5 mm) and for manipulation of multiplanar views. Images were scored by two radiologists independently with 3 (KDP, Observer 1) and >20 years (NdS, Observer 2) of experience in pelvic imaging, respectively. The quality of the images was scored as high (=2), medium (=1), or low (=0). The sciatic nerve was chosen as the reference structure as it is the largest nerve bundle in the pelvis, stable in position, and therefore a good landmark. High-quality images would allow the definition of at least eight individual nerve roots within the fibular and tibial trunks combined of the sciatic nerve (Fig. 2); medium-quality images allowed for sharp definition of <8 nerve roots; poor-quality images were defined as blurry images, in which no separate nerve roots could be defined. In every participant, each observer scored the visibility of the main autonomic plexuses (namely the superior hypogastric plexus [SHP], left/right hypogastric nerves, inferior hypogastric plexus [IHP], and somatic nerves [left/right sciatic and pudendal nerves]). Their conspicuity was graded as: 0 = not seen; 1 = poorly seen; or 2 = well

seen. Subsequently, observational agreement in percentage scored identically in terms of image quality and nerve identification was recorded. As there was a large imbalance in the classes graded, it was not possible to calculate kappa meaningfully.

Results

Pelvic nerves in comparison to their known anatomical course

Autonomic nerves. A schematic drawing of the autonomic pelvic innervation and corresponding MR images is shown in Fig. 3. The SHP was identified anteriorly to the fifth lumbar vertebral body–sacral promontory in 19/20 cases by Observer 1, while Observer 2 identified the SHP in 18/20 cases (Table 2, Fig. 4). The SHP is mainly supplied by branches of the sympathetic chains in addition to parasympathetic splanchnic nerves and gives rise to two plexiform structures—the hypogastric nerves—i.e. a sheath or mesh of nerves to both sides of the pelvis, which course along the common iliac chains. The hypogastric nerves were identified connecting the SHP and IHP. Like the SHP, they were detected in 95% and 90% by Observer 1 and Observer 2, respectively (Table 1).

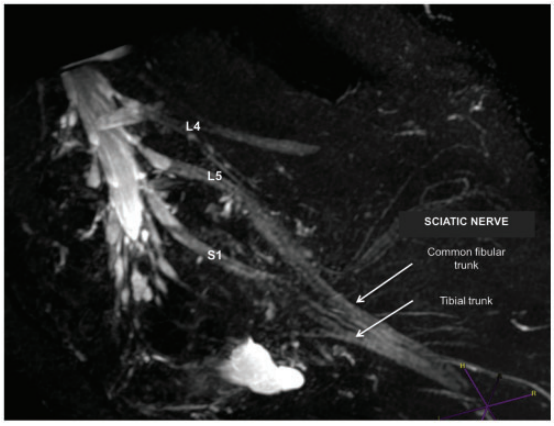

Fig. 2. Image quality assessment based on the conspicuity of the individual fibers of the sciatic nerves. Identification of ≥8 individual fibers indicated high quality, <8 indicated medium quality, and images were regarded as low quality if no individual fiber could be depicted.

The IHP was identified well in 85% (34/40) of cases by Observer 1 and in 75% (30/40) by Observer 2 (Table 2, Fig. 5). It is made up of the convergence of the hypogastric nerves and the splanchnic nerves originating from the sacral roots (mainly S2 and S3). This plexus is situated medially to the internal iliac vessels and has a triangular form with the base oriented posteriorly and the top of the triangle at the point where the ureter enters the posterior broad ligament. Distal to the IHP, the fan out of the plexus laterally and medially into the vesical and rectovaginal plexus, respectively, was beyond the resolution of the MR images due to the small diameter of these nerves.

Somatic nerves. The lumbosacral nerve roots were followed in 3D on their exit from their nerve root foramina to identify the pelvic somatic nerves. The sciatic nerve was first identified from its L4-S3 roots and was well seen in all cases (100% Observer 1 and Observer 2). The superior gluteal (L4-S1) and inferior gluteal (L5-S2) nerves were considered outside the pelvis and were not part of this analysis. The pudendal

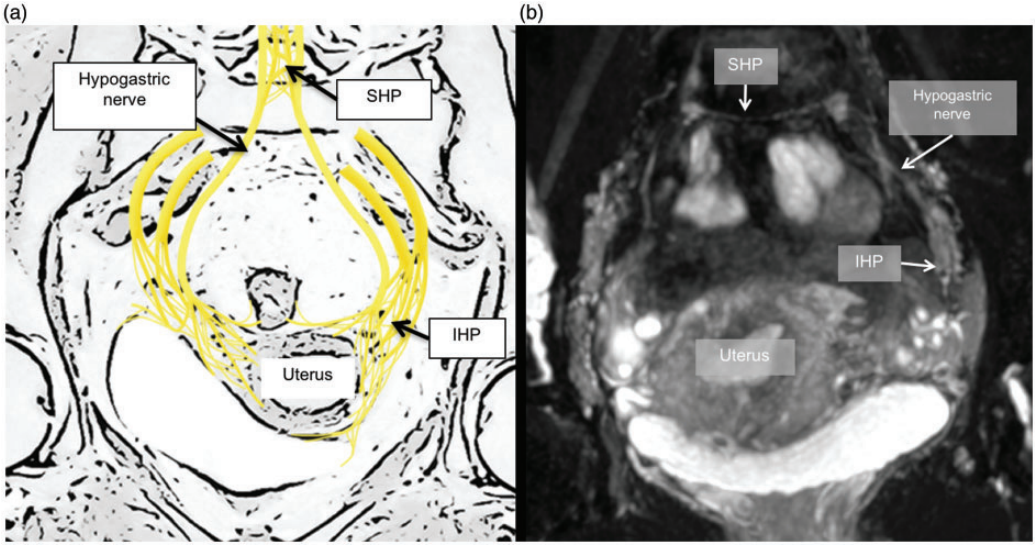

Fig. 3. Coronal schematic drawing of the autonomic pelvic plexus (a) and the corresponding NerveVIEW image (b).

Table 2. Comparison of pelvic nerve conspicuity between two observers for all participants.

Nerves assessed	Nerves scored by Observer 1			Nerves scored by Observer 2			Inter-observer agreement (%)
	Well-identified (2)	Poorly identified (1)	Not identified (0)	Well-identified (2)	Poorly identified (1)	Not identified (0)	
Superior hypogastric plexus	10/20 (50)	9/20 (45)	1/20 (5)	10/20 (50)	8/20 (40)	2/20 (10)	12/20 (60)
Hypogastric nerves	20/40 (50)	18/40 (45)	2/40 (5)	20/40 (50)	18/40 (40)	4/40 (10)	24/40 (60)
Inferior hypogastric plexus left	18/20 (90)	2/20 (10)	0/20 (0)	17/20 (85)	3/20 (15)	0/20 (0)	15/20 (75)
Inferior hypogastric plexus right	16/20 (80)	4/20 (20)	0/20 (0)	13/20 (65)	6/20 (30)	1/20 (5)	12/20 (60)
Sciatic nerve left	20/20 (100)	0/20 (0)	0/20 (0)	20/20 (100)	0/20 (0)	0/20 (0)	20/20 (100)
Sciatic nerve right	20/20 (100)	0/20 (0)	0/20 (0)	20/20 (100)	0/20 (0)	0/20 (0)	20/20 (100)
Pudendal nerve left	13/20 (65)	7/20 (35)	0/20 (0)	16/20 (80)	4/20 (20)	0/20 (0)	13/20 (65)
Pudendal nerve right	13/20 (65)	7/20 (35)	0/20 (0)	13/20 (65)	7/20 (35)	0/20 (0)	14/20 (70)

Values are given as n (%).

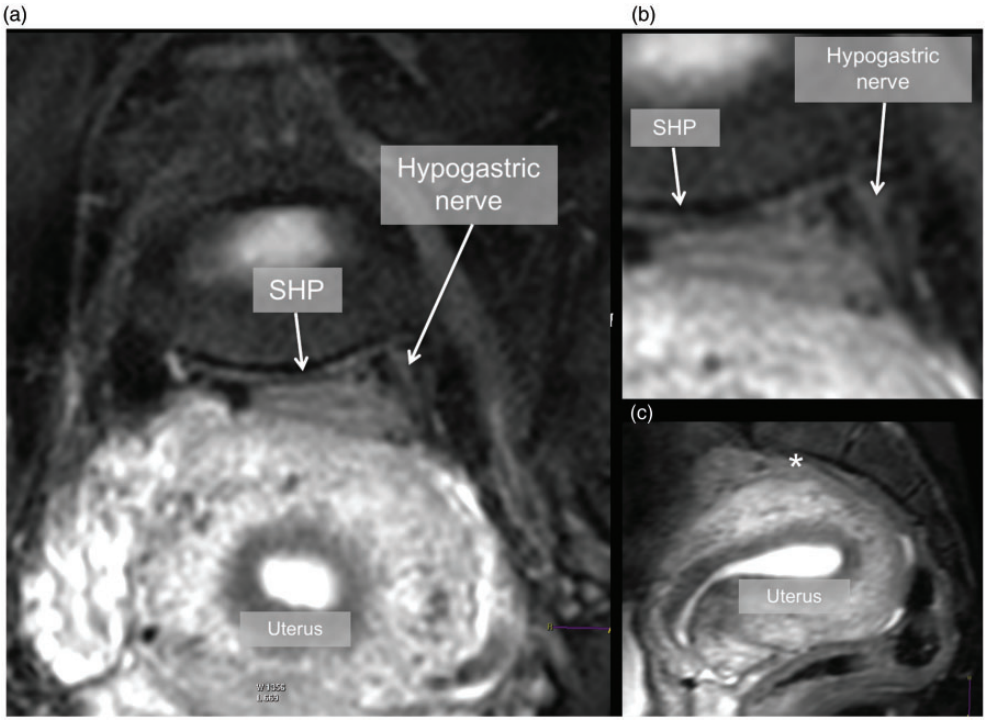

Fig. 4. Coronal NerveVIEW image (a) shows band-like configuration of the SHP and the proximal part of the hypogastric nerve, which is better appreciated on the enlarged image (b). (c) The typical presacral location of the SHP (*).

plexus (S2-S4), which provides the major sensory and motor innervation of the muscles of the perineum and the pelvic floor, including the somatic innervation of the external urethral and anal sphincter, was followed as it runs from the spine (Fig. 6) through the greater sciatic foramen and exits the pelvis through the lesser sciatic foramen. The pudendal nerve was identified as it courses through the pudendal canal (Alcock's canal), formed by the obturator fascia. It was well seen in 65% (26/40) of cases by Observer 1 and in 72.5% (29/40) of cases by Observer 2 (Table 2). Branches into an inferior rectal branch supplying the external anal sphincter, and a perineal nerve supplying the deep perineal muscles and the external urethral sphincter, were too small to visualize reliably and were not formally evaluated.

Inter-observer analysis

Images of all participants were of medium to high quality according to both observers and scores agreed in 75% (15/20 participants).

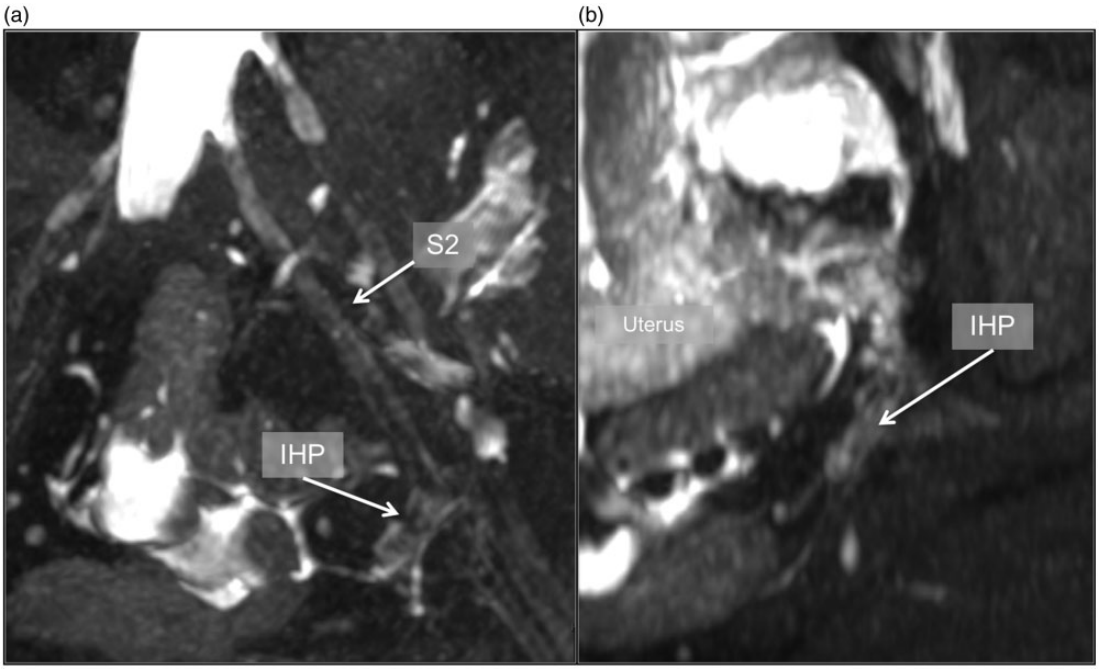

Fig. 5. Coronal NerveVIEW image (a) demonstrates the sacral nerve root S2 branching into the inferior hypogastric plexus (IHP) and the corresponding axial image showing the IHP (b).

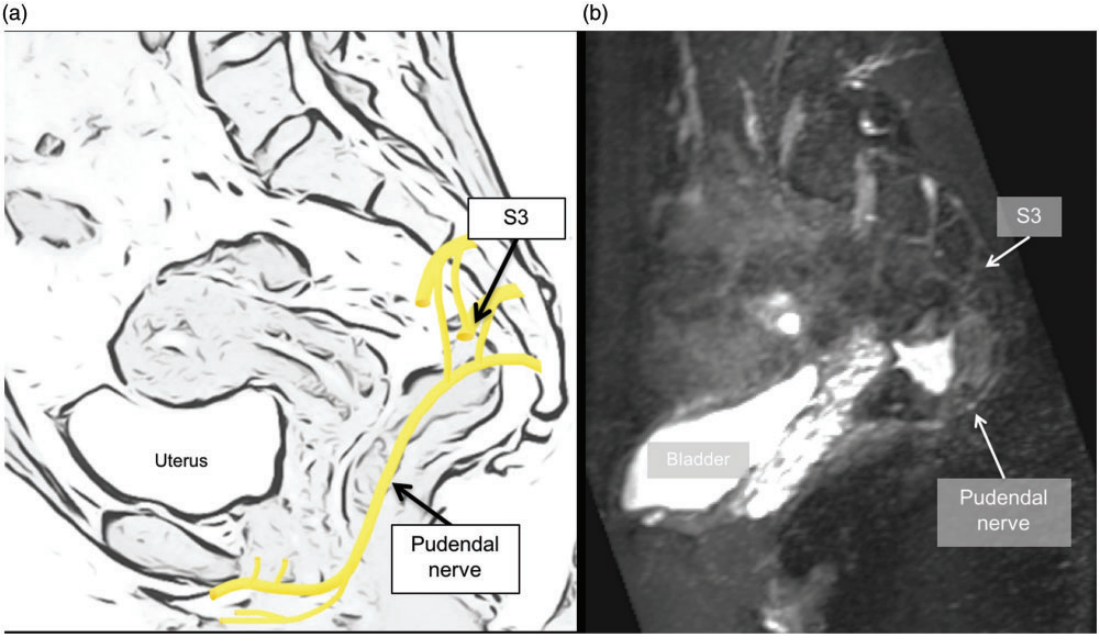

Fig. 6. Sagittal schematic drawing of the pudendal nerve (a) and the corresponding NerveVIEW image (b).

Scores for autonomic and somatic nerve conspicuity for each observer are summarized in Table 2. Overall, 72.2% (130/180) of nerves/plexuses were clearly seen by Observer 1 and 71.7% (129/180) by Observer 2 with an inter-observer agreement of 71.7% (130/140). Agreement between observers for autonomic nerves was 60% (36/60) for SHP and hypogastric nerves, and 67.5% (27/40) for IHP. Agreement of somatic nerve conspicuity was 83.8%, and 100% for the sciatic nerves (40/40) and 67.5% (27/40) for pudendal nerves.

There was no difference in nerve detection between volunteers and patients. In the volunteer cohort, image quality was graded high in 74.1% (40/54 nerves) and 64.8% (35/54) by Observer 1 and Observer 2, respectively; corresponding values for the patient cohort were 71.4% (90/126) and 74.6% (94/126). Agreement on nerve conspicuity scoring between observers was 66.7% (36/54) for the volunteers and 74.6% (94/126) for the patients.

Discussion

The present study demonstrates that a modified 3D NerveVIEW sequence enables the visualization of the larger autonomic pelvic plexuses and somatic nerves supplying the female pelvis with good inter-observer agreement. Identification of the pelvic splanchnic nerves and smaller branches of the autonomic nerves to the uterus, vagina, and bladder were beyond the resolution of the current technique and may benefit from further post-processing as recently demonstrated (15).

Traditional MRN protocols consist of conventional T2 and T1 sequences, a 3D TSE sequence with fat suppression, and 3D balanced gradient echo steady-state precession sequence with diffusion-weighted imaging (DWI) (17). MRN of the pelvic nerves, particularly the plexuses, poses specific challenges as multiple factors generate a significant decrease in the signal-to-noise ratio (SNR) such as a preponderance of fat on fat-suppressed images and artefacts induced by vascular pulsation and bowel peristalsis, while covering a large FOV (18). Furthermore, due to their size and anatomy, the autonomic pelvic plexuses are difficult to discriminate from the pelvic organs and adjacent vascular plexuses. Therefore, the two major challenges in sequence optimization were achieving adequate and homogenous fat suppression and canceling the confounding signal of adjacent vessels. To achieve adequate fat suppression, STIR was applied rather than SPectral Attenuated Inversion Recovery (SPAIR) as the former resulted in a more robust fat suppression due to a lower sensitivity for field inhomogeneities (19,20), which is further improved by the application of adiabatic pulses to create a more homogenous field (16,21). In the present study, increased effectiveness of the STIR pulse was achieved by the use of the OIT pulse for inversion. The application of MDSE is a relatively recent development in MRN and has been assessed in the brachial plexus by Klupp et al. (22) and in the lumbar plexus by Kasper et al. (23). In agreement with their work, we found that the use of MDSE provided high-quality images with good fat and vessel suppression, which was also improved by the use of OIT radiofrequency pulses for the MSDE refocusing. Another measure to ensure adequate signal suppression of the pelvic venous plexus was by setting the velocity encoding equivalent to the blood flow velocity. In addition, to minimize confounding factors, the SNR of the nerves themselves was improved using a tissue-specific refocusing FA modulation. This enabled the shaping of the signal intensity along the echo train, achieving high signal and reduced blurring for pelvic nerves. This approach is routinely part of traditional (13) and newer MRN sequences such as SHINKEI (23). Cervantes et al. (24) pointed out that careful optimization of the refocusing FA design reduces blurring effects and could improve the detection of smaller nerves.

The literature on MRN in the pelvis is limited. In line with Delaney et al. (14) and Soldatos et al. (13), we found that the sciatic nerve was well seen with clear depiction of the individual fibers. The proximal pudendal nerve could be clearly followed up into Alcock's canal, while the distal pudendal nerves were too small to be confidently identified, which is in line with the findings of Chhabra et al. (25).

However, the novelty and added value of the modified 3D NerveVIEW technique developed in our study is its ability to show the autonomic pelvic plexuses such as the SHP and IHP. A previous cadaveric study by Mauroy et al. (26) related different anatomic cuts to different planes or "cuts" on a conventional T2 MRI sequence, but the location of the different pelvic plexus components was suggested, rather than actually demonstrated on the images. One other ex vivo study (27) segmented pelvic autonomic nerves and organs on MR images using dedicated software and found good correlation between MRI and the surgical dissection findings. In concurrence with their research, a recent in vivo study (15) demonstrated the feasibility of 3D reconstruction of female pelvic autonomic nerves after semi-automatic nerve segmentation. A 3D STIR sequence was applied allowing for the reconstruction of the SHP in 100% of cases, of the hypogastric nerves in 96.7%, and the IHP in 93.3% of cases, which is comparable to the detection rate of the pelvic autonomic nerves demonstrated in the current study. Similar to their findings, we also found the SHP to be easier to detect than the IHP, probably due its relatively fixed presacral position and paucity of surrounding confounding structures. Both the studies by Li et al. (15) and Bertrand et al. (27) focused on computer-aided segmentation and 3D reconstruction of the pelvic autonomic nerves. Therefore, expected disadvantages were the long analysis time and the need to develop or purchase dedicated software. In the current study, we showed that pelvic somatic and autonomic pelvic innervation can reliably be identified based on direct visual analysis and may therefore be easier to implement in routine pelvic MRI examinations.

Our study had several limitations. First, the autonomic nerve plexuses could only be recognized on the MIP image with a slab thickness of 3 mm. Therefore, determining the exact position of these nerves in relation to the pelvic organs requires co-registration of the MRN images with high-resolution 3D T1 or T2 images. Second, despite all the measures to suppress the vascular signal, differentiation between vessels and nerves was imperfect and required careful image assessment, meticulously following the nerve course form the spinal canal to the periphery by scrolling through the image stack. We found that nerves had a smoother aspect and returned a slightly less hyperintense signal than the neighboring vessels. We did not scan volunteers in the first half of their menstrual cycle, which might reduce pelvic congestion, although this was not found to be a limiting factor for nerve delineation. Third, the current patient cohort also included patients with cervical pathology. However, in all patients, disease was limited without involving the neurovascular plexuses.

In conclusion, using a modified 3D NerveVIEW protocol rendered high-quality nerve images and enabled reproducible depiction of the autonomic and somatic nerves in the female pelvis with good inter-observer agreement on image quality and nerve conspicuity. Future studies will have to investigate whether the more detailed depiction of the pelvic anatomy with MRN can assist in planning of the treatment of pelvic malignancies.

Declaration of conflicting interests

The author(s) declared no potential conflicts of interest with respect to the research, authorship, and/or publication of this article.

Funding

The author(s) disclosed receipt of the following financial support for the research, authorship, and/or publication of this article: CRUK and EPSRC support to the Cancer Imaging Centre at ICR and RMH in association with MRC and Department of Health C1060/A10334, C1060/A16464 and NHS funding to the NIHR Biomedical Research Centre and the Clinical Research Facility in Imaging.

ORCID iDs

Katja N De Paepe https://orcid.org/0000-0002-2891-7545
Nandita M deSouza https://orcid.org/0000-0003-4232-476X

References

1. Rob L, Halaska M, Robova H. Nerve-sparing and individually tailored surgery for cervical cancer. Lancet Oncol 2010;11:292–301.
2. Sakuragi N, Todo Y, Kudo M, et al. A systematic nerve-sparing radical hysterectomy technique in invasive cervical cancer for preserving postsurgical bladder function. Int J Gynecol Cancer 2005;15:389–397.
3. Fujii S, Takakura K, Matsumura N, et al. Anatomic identification and functional outcomes of the nerve sparing Okabayashi radical hysterectomy. Gynecol Oncol 2007;107:4–13.
4. Kuponiyi O, Alleemudder DI, Latunde-Dada A, et al. Nerve injuries associated with gynaecological surgery. Obstet Gynaecol 2014;16:29–36.
5. Cardosi RJ, Cox CS, Hoffman MS. Postoperative neuropathies after major pelvic surgery. Obstet Gynecol 2002;100:240–244.
6. Butler-Manuel SA, Buttery LDK, Polak JM, et al. Autonomic nerve trauma at radical hysterectomy: the nerve content and subtypes within the superficial and deep uterosacral ligaments. Reprod Sci 2008;15:91–96.
7. Butler-Manuel SA, Buttery LDK, A'Hern RP, et al. Pelvic nerve plexus trauma at radical and simple hysterectomy: a quantitative study of nerve types in the uterine supporting ligaments. J Soc Gynecol Investig 2002;9:47–56.
8. Butler-Manuel SA, Buttery LD, A'Hern RP, et al. Pelvic nerve plexus trauma at radical hysterectomy and simple hysterectomy: the nerve content of the uterine supporting ligaments. Cancer 2000;89:834–841.
9. Todo Y, Kuwabara M, Watari H, et al. Urodynamic study on postsurgical bladder function in cervical cancer treated with systematic nerve-sparing radical hysterectomy. Int J Gynecol Cancer 2006;16:369–375.
10. Castiglione F, Bergamini A, Albersen M, et al. Pelvic nerve injury negatively impacts female genital blood flow and induces vaginal fibrosis-implications for human nerve-sparing radical hysterectomy. BJOG 2015;122:1457–1465.
11. Sagebiel TL, Viswanathan C, Patnana M, et al. Overview of the role of imaging in pelvic exenteration. Radio Graphics 2015;35:1286–1294.
12. Llewelyn M, Wells E, Taylor A. PO-0865: Developing sciatic nerve-sparing stereotactic radiotherapy for re-irradiating the pelvic sidewall. Radiother and Oncol 2016;119:S413.
13. Soldatos T, Andreisek G, Thawait GK, et al. High-resolution 3-T MR neurography of the lumbosacral plexus. RadioGraphics 2013;33:967–987.
14. Delaney H, Bencardino J, Rosenberg ZS. Magnetic resonance neurography of the pelvis and lumbosacral plexus. Neuroimaging Clin N Am 2014;24:127–150.
15. Li P, Liu P, Chen C, et al. The 3D reconstructions of female pelvic autonomic nerves and their related organs based on MRI: a first step towards neuronavigation during nerve-sparing radical hysterectomy. Eur Radiol 2018;28:4561–4569.
16. Tannús A, Garwood M. Adiabatic pulses. NMR Biomed 1997;10:423–434.
17. Chhabra A, Lee PP, Bizzell C, et al. 3 Tesla MR neurography—technique, interpretation, and pitfalls. Skeletal Radiol 2011;40:1249–1260.
18. Rafat Zand K, Reinhold C, Haider MA, et al. Artifacts and pitfalls in MR imaging of the pelvis. J Magn Reson Imaging 2007;26:480–497.

19. Qayyum A. Diffusion-weighted imaging in the abdomen and pelvis: concepts and applications. RadioGraphics 2009;29:1797–1810.
20. Sensakovic WF. Regarding fat suppression in MRI, when are spectral techniques preferred over STIR, and vice versa? AJR Am J Roentgenol 2015;205: W231–W232.
21. Rosenfeld D, Panfil SL, Zur Y. Design of adiabatic pulses for fat-suppression using analytic solutions of the Bloch equation. Magn Reson Med 1997;37:793–801.
22. Klupp E, Cervantes B, Sollmann N, et al. Improved brachial plexus visualization using an adiabatic iMSDE-Prepared STIR 3D TSE. Clin Neuroradiol 2019;29:631–638.
23. Kasper JM, Wadhwa V, Scott KM, et al. SHINKEI—a novel 3D isotropic MR neurography technique: technical advantages over 3DIRTSE-based imaging. Eur Radiol 2015;25:1672–1677.
24. Cervantes B, Bauer JS, Zibold F, et al. Imaging of the lumbar plexus: Optimized refocusing flip angle train design for 3D TSE. J Magn Reson Imaging 2016;43: 789–799.
25. Chhabra A, McKenna CA, Wadhwa V, et al. 3T magnetic resonance neurography of pudendal nerve with cadaveric dissection correlation. World J Radiol 2016;8:700.
26. Mauroy B, Demondion X, Bizet B, et al. The female inferior hypogastric (=pelvic) plexus: anatomical and radiological description of the plexus and its afferences–applications to pelvic surgery. Surg Radiol Anat 2007;29:55–66.
27. Bertrand MM, Macri F, Mazars R, et al. MRI-based 3D pelvic autonomous innervation: a first step towards image-guided pelvic surgery. Eur Radiol 2014;24:1989–1997.